Preprint, published in Journal of Pressure Vessel Technology, April 2019, 021301- 1, 021302-11.
DOI: 10.1115/1.4042799

Impulsive Motion in a Cylindrical Fluid-Filled Tube Terminated by a Converging Section

Jean-Christophe Veilleux and Joseph E. Shepherd
Graduate Aerospace Laboratories
California Institute of Technology
Pasadena, California 91125
Email: jc.veilleux@caltech.edu

The syringe in a subcutaneous autoinjector may be subjected to internal pressure transients due to the normal operation of the injection mechanism. These transients are similar to transients in fluid-filled pipelines observed during water hammer events. In this paper, the effect of an air gap in the syringe and a converging section are studied experimentally and numerically in a model system which consists of a fluid-filled metal tube that is impulsively loaded with a projectile to simulate the action of the autoinjector mechanism operation.

The air between the buffer and the water results in a complex interaction between the projectile and the buffer. Also, there are tension waves inside the tube due to the presence of a free surface and the motion of the buffer, and this causes distributed cavitation which, in turn, gives rise to steepening of the pressure waves. The converging section can amplify the pressure waves if the wave front is sharp, and it can enhance the collapse of bubbles. Pressures as high as 50 MPa have been measured at the apex of the cone with impact velocities of 5.5 m/s.

1 Introduction

Autoinjectors are now ubiquitous in the pharmaceutical industry. These devices are both used with drugs to be administered in case of emergency (e.g., epinephrine), and with drugs to be administered on a frequent basis (e.g., etanercept, adalimumab and darbepoetin alfa) [1]. The popularity of autoinjectors is in part due to the compactness and the ease of use of the devices [2,3], and to a trend toward large molecule drugs that cannot be administered orally [4–6].

Although the specific design of each autoinjector may differ, in most devices currently available on the market, the mechanism is spring actuated [4, 6, 7]. Activation of the autoinjector results in mechanical impacts between the moving components of the mechanism [8]. This can be an issue when very viscous drugs are to be injected since the large spring forces needed can result in failure of the device [8–10].

The filling process of the syringe typically results in an air bubble within the syringe. In the vertical, tip-down orientation considered in this paper, the air bubble is located between the plunger stopper and the drug solution. The presence of an air gap has a significant effect on the transient events upon device actuation [8].

The pressure transients inside the syringe have been experimentally measured by Veilleux and Shepherd [8]. The results suggest the transients are similar to those observed in fluid-filled pipelines during water hammer events [11–14]. Inaba and Shepherd [15, 16] examined pressure transients which are closely related to the present work.

There are four main differences between these previous studies and the syringe situation: 1) the mechanism of initiating the transient; 2) the air gap; 3) the converging section; 4) the translational motion of the syringe. The aim of this paper is to use experimental measurements and numerical simulations to investigate and explain the effect of these features on measured pressure and strains, except for the translational motion (item 4): the syringe model is static in this work. The effect of the translational motion is important, but it is not discussed in this paper; this will be reported in a separate publication.

2 Experimental Setup

A schematic of the experimental setup is shown in Fig. 1. Note that the z-axis, or longitudinal axis, is defined downward positive, and all distances are relative to the top end of the aluminum tube. The experimental apparatus consists of three main components: the guide tube, the projectile, and the test specimen.

The guide tube – inner diameter of 50.8 mm and length of approximately 2.1 m – is only partially shown in Fig. 1. The purpose of this tube is to guide the projectile while it is vertically accelerated to velocities up to 6.4 m/s using gravity alone. The projectile consists of a 0.5 kg aluminum cylinder – 50.7 mm in diameter and 102 mm in length – which can slide freely within the guide tube.

The test specimen consists of a thick-wall aluminum tube with a length of 0.91 m, an outer diameter of 50.8 mm, and an inner diameter of 38.1 mm. The tube is filled with

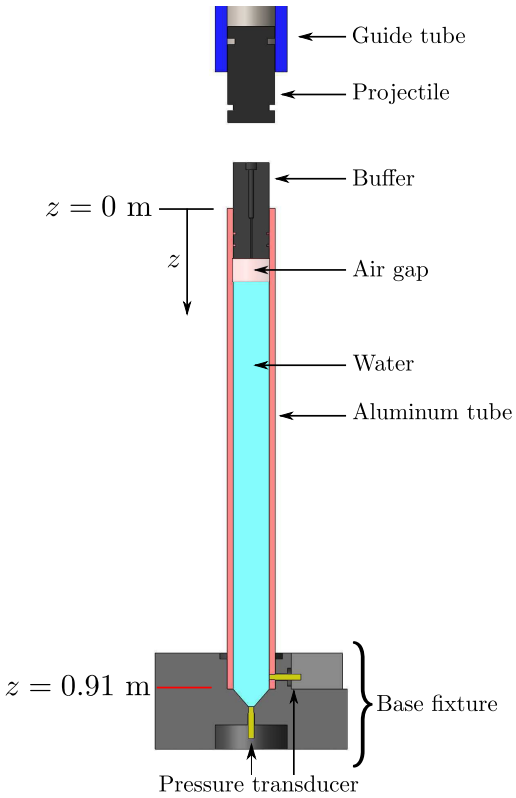

Fig. 1: Schematic of the experimental setup.

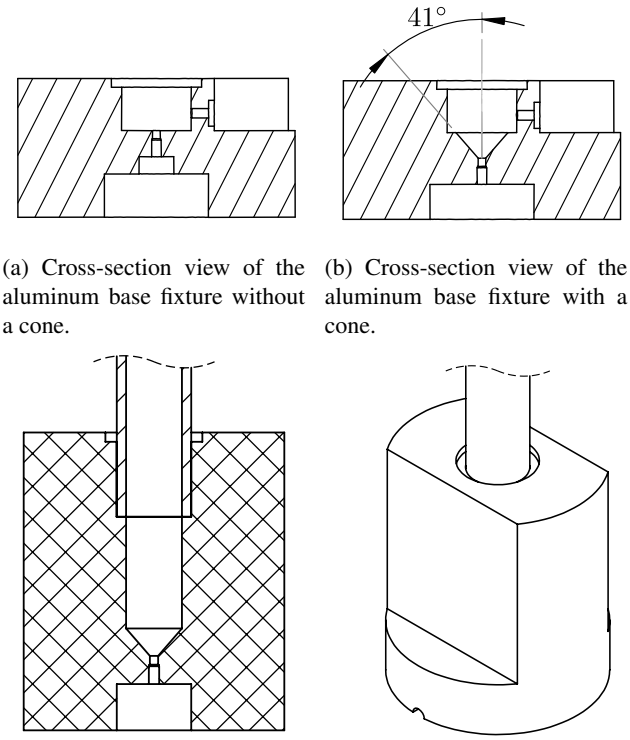

(a) Cross-section view of the aluminum base fixture without a cone.

(b) Cross-section view of the aluminum base fixture with a cone.

(c) Cross-section view (left) and isometric view (right) of the polycarbonate base fixture with a partial view of the aluminum tube.

Fig. 2: Schematic of the base fixtures (single hatch for aluminum, and double hatch for polycarbonate).

de-ionized water[1], and it is mounted into a cylindrical base fixture which is bolted to heavy plates resting on the ground (not shown). The overall mass of the test specimen, including the base fixture and the plates, is over 50 kg.

The three base fixtures shown in Fig. 2 were used. The first two base fixtures (Figs. 2a and 2b) were fabricated using aluminum. The aluminum tube was positioned into the base fixture as shown in Fig. 1, and it was secured in place using a shrink fit. In the first geometry (Fig. 2a) the bottom of the aluminum tube is terminated with a flat end perpendicular to the longitudinal axis z. In the second geometry (Fig. 2b) the aluminum tube is terminated with a conical section similar to that of a syringe. The half-angle of the cone is 41°. In both geometries there are two ports for mounting piezoelectric pressure transducers. Note that the half-angle of the cone can have a local effect on the pressure and strains; our investigation of the effect of cone shape will be reported in a future publication.

The third base fixture (Fig 2c) was fabricated using optically-clear polycarbonate. The polycarbonate was vapor polished after machining to ensure optical clarity of the final product. This fixture is taller because it contains a 76 mm long straight section of tube terminated with a 41° cone. The aluminum tube was positioned into the base fixture as shown in Fig. 2c, and it was secured using epoxy. The aluminum tube was shortened by 76 mm to make sure the overall distance between the top end of the tube and the entrance of the cone is 0.91 m as for the other two base fixtures. The third base fixture makes it possible to observe the water and cavitation within the cone and the last 76 mm of straight tube.

Table 1: Axial location of the pressure transducers.

Transducer	**Without the cone**	**With the cone**
P1	895 mm	895 mm
P2	910 mm	927 mm

The pressure transducers mounted into the base fixtures are also shown in Fig. 1. The precise locations of the transducers are indicated in Tab. 1. For the aluminum base fixture which has a conical section, one transducer is located above the converging section and the other one is positioned at the apex of the conical section. Note that the polycarbonate base fixture only has one port for mounting a pressure transducer, and it is located at the apex of the cone.

The test specimen is sealed at its top end using a 104 mm long polycarbonate cylinder used as a buffer between the projectile and fluid. There are two O-rings between the buffer and the aluminum tube for sealing. There is a small hole along the longitudinal axis of the buffer which is closed using a socket screw before an experiment. This opening allows for the introduction of an air gap of controlled size between the bottom end of the buffer and the water contained

[1]Several experiments were performed with degassed, de-ionized water (not reported in this paper). This did not alter the results significantly.

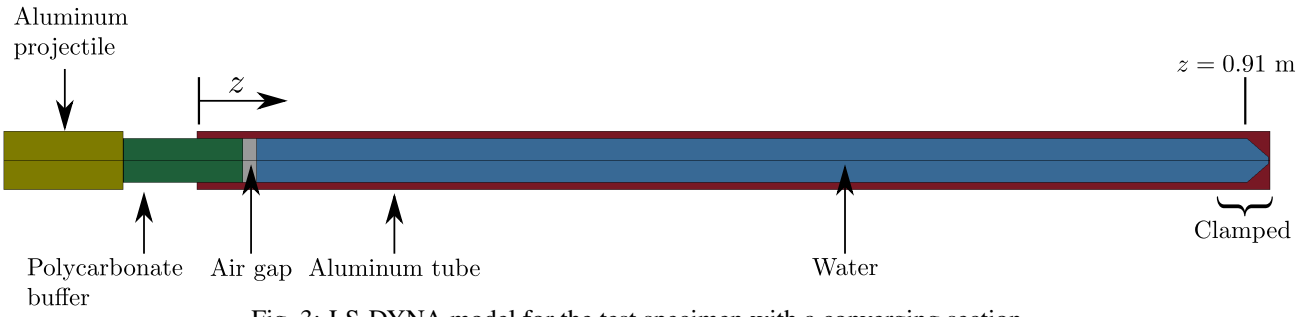

Fig. 3: LS-DYNA model for the test specimen with a converging section.

Table 2: Axial location of the strain gauges.

Station	S1	S2	S3	S4	S5	S6	S7
z (mm)	127	254	381	508	635	762	857

in the tube as shown in Fig. 1. For all cases reported in this paper, the bottom end of the buffer is located at $z = (51 - d_0)$ mm, where d_0 is the initial air gap size.

In addition to the pressure sensors (PCB 113A23) there are 14 strain gauges to measure the hoop and axial strains at 7 axial locations on the outer wall of the aluminum tube. The strain gauges are a combination of Vishay CEA-06-125UN-350/P2 and HBM K-LY4-3-05-350-3-2. The location of each gauge is indicated in Tab. 2. Note that no strain gauge is installed at station S7 with the polycarbonate base fixture.

A high-speed video camera (Vision Research Phantom V7.0G) is used to visualize the contact between the projectile and the buffer, making it possible to track the projectile and the buffer to study their interaction and to measure the impact velocity. When using the polycarbonate base fixture, a second high-speed video camera (Vision Research Phantom V1612) is used to visualize the cavitation events within the visible section of the tube and cone.

The analogy between the test setup and an actual autoinjector is as follows: the projectile corresponds to the spring actuated plunger rod, the buffer corresponds to the plunger-stopper, the aluminum tube corresponds to the glass syringe and the water corresponds to the drug solution. Note that the acoustic impedance of aluminum (1.5×10^7 kg·m^{-2}s^{-1}) and the acoustic impedance of borosilicate glass (1.3×10^7 kg·m^{-2}s^{-1}) are similar, effectively making the acoustic response of the large scale model similar to the acoustic response of a pre-filled, glass syringe.

The use of water rather than a viscous drug solution in the syringe is justified because the viscous effects are negligible during the transient events examined in this report. This is because at the time scale of interest, less than 5 ms, there is no flow through the needle or syringe. The establishment of a flow through the needle and syringe occurs much later. The effect of fluid viscosity on the wave dynamics is small during the initial transient because the gradients in velocity and the motion of the fluid elements correspond to acoustic disturbances with small amplitude.

3 Numerical Simulation

The numerical simulations have been performed using LS-DYNA [17], a general-purpose finite element code which can model fluid-structure interaction. The geometry of the LS-DYNA model is shown in Fig. 3. The model is 2D axysimmetric, and the mesh is constructed using Lagrangian shell elements. All components are meshed using a structured grid except for the conical section. The elements are approximately 0.5 mm $\times$ 0.5 mm in size unless otherwise indicated, and this yields a total of $\approx$110,000 elements. A Courant number of 0.5 was used in all simulations.

The projectile, buffer, air gap, water and wall are all modeled as separate material regions or parts. The base fixture is not modeled and is approximately taken into account through a boundary condition; the nodes of the wall which would be in contact with the base fixture are all rigidly clamped. The elements forming the air gap are also constrained to avoid getting a highly distorted mesh; they can only deform axially.

The nodes at the buffer-air gap interface are shared by the two components. The same is true about the nodes at the air gap-water interface. For the cases where no air gap is present, the nodes at the buffer-water interface are shared by both parts. By sharing the nodes between two parts no contact model is needed.

At the projectile-buffer interface and at the water-wall interface, the LS-DYNA built-in surface-to-surface contact model is used [17]. This contact model does not apply forces in the tengential direction (i.e., the elements can slip). In fact, this contact model can only account for compression between the two surfaces; tensile forces are not transmitted between the two surfaces such that the cavitation inception pressure corresponds to zero absolute pressure. In this model, whenever the liquid experiences tension, there is a loss of contact between the water and the wall, mimicking cavitation. The formation of the voids forces the pressure to remain at or above zero absolute pressure. The growth and the collapse of those voids locally mimic the effect of the bubbles during cavitation.

A linear-elastic constitutive model is used for all solid parts. A Mie-Grüneisen equation of state [18] is used for the water. The gas in the air gap is an isentropically compressed

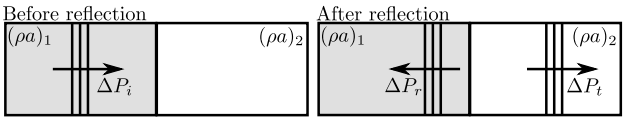

Fig. 4: Reflection of pressure waves at an interface.

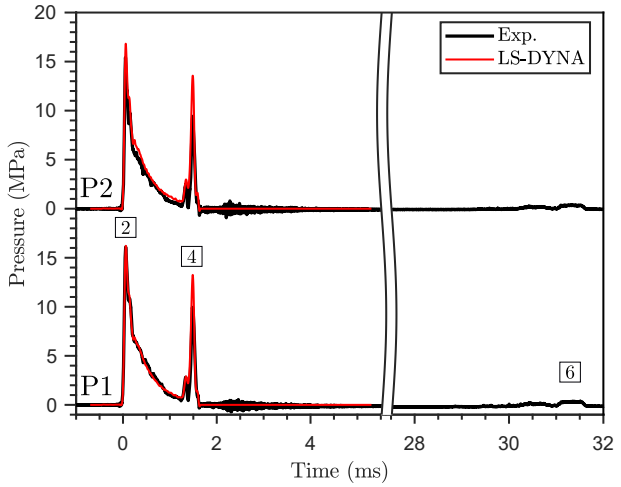

Fig. 5: Pressure at the bottom end for case 1 (the time axis is discontinuous).

perfect gas (i.e., $P/\rho^\gamma = \text{constant}$)[2].

Initially, all components are at rest except for the projectile which is traveling at the impact velocity V_0. The projectile and the buffer are initially a small distance apart (0.1 mm). Gravity is not accounted for in the simulations. It was verified that further refinement of the grid and the time step by a factor of 4 does not affect the results significantly. Finally, all simulations are terminated shortly after the onset of cavitation due to the absence of an explicit cavitation model in the model.

4 Results

Five cases are reported in this paper to illustrate the effect of an air gap and a converging section:

Case 1: no converging section, no air gap;
Case 2: with a converging section, no air gap;
Case 3: no converging section, 3.5 mm air gap;
Case 4: no converging section, 12 mm air gap;
Case 5: with a converging section, 12 mm air gap.

4.1 Case 1

The first case considered is the simplest configuration with no air gap and no cone. The water column is pressurized through a direct contact between the buffer and the liquid; the liquid at the interface is forced to move with the buffer. The

[2]Aluminum: ρ = 2712 kg/m^3, E = 69.6 GPa, ν = 0.33, a = 5500 m/s. Polycarbonate: ρ = 1200 kg/m^3, E = 2.6 GPa, ν = 0.37, a = 2270 m/s. Water: ρ_0 = 1000 kg/m^3, a = 1500 m/s, S_1 = 0, S_2 = 0, S_3 = 0,γ_0 = 0. Air: γ = 1.4.

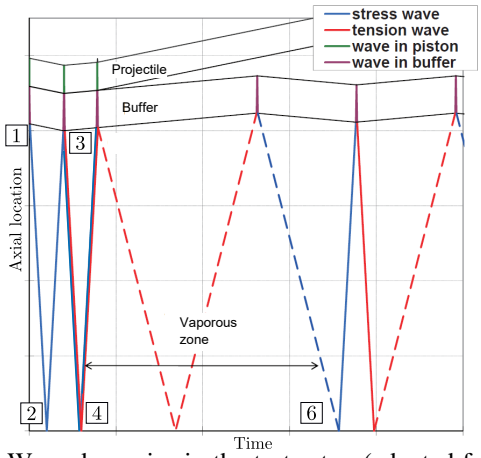

Fig. 6: Wave dynamics in the test setup (adapted from [15] with permission).

measured impact velocity of the projectile on the buffer is 5.7 m/s.

This configuration was examined previously by Inaba and Shepherd [15], but without the base fixture used in the present study. Another difference is that Inaba and Shepherd used a polycarbonate tube instead of an aluminum tube. As a result, the coupling between the liquid and the structure was substantially more important than in the present study. Despite the differences, the wave dynamics described in detail by Inaba and Shepherd are essentially the same as in the present study.

Because there are many reverberations of the stress waves within the projectile and the buffer during the slowing of the buffer, the projectile and buffer can be treated as rigid bodies. The transit time of the stress waves is 36 μs in the projectile and 44 μs in the buffer; this is shorter than the rise time of the pressure, approximately 75-100 μs. The idea that the motion of the projectile and the buffer is governed by rigid body mechanics has been validated through numerical simulations; making the buffer and the projectile rigid does not change the results other than producing a small increase of the peak pressures. This is of course a simplifying assumption, and the reader should see [19] for a more detailed treatment of stress wave dynamics in the projectile and buffer.

The maximum pressure in the liquid below the buffer can be estimated using acoustic theory [20]. Assuming the initial velocity of the buffer is the impact velocity V_0, $P_{max} \approx \rho a V_0$ and this yields a value of 8.55 MPa. As discussed in [16], we expect this pressure increase to be followed by an exponential decay since the buffer begins slowing down immediately after impact, thus creating expansion waves which follow the initial compression wave.

Pressure transducers P1 and P2 are located very close to the bottom wall where the wave reflects, as a consequence measured peak pressure is larger than 8.55 MPa. When the wave reaches the bottom wall, it will be partly transmitted through the base fixture and partly reflected into the water. The reflected pressure ΔP_r is determined by the acoustic impedances (ρa) of the materials at the interface (see Fig. 4),

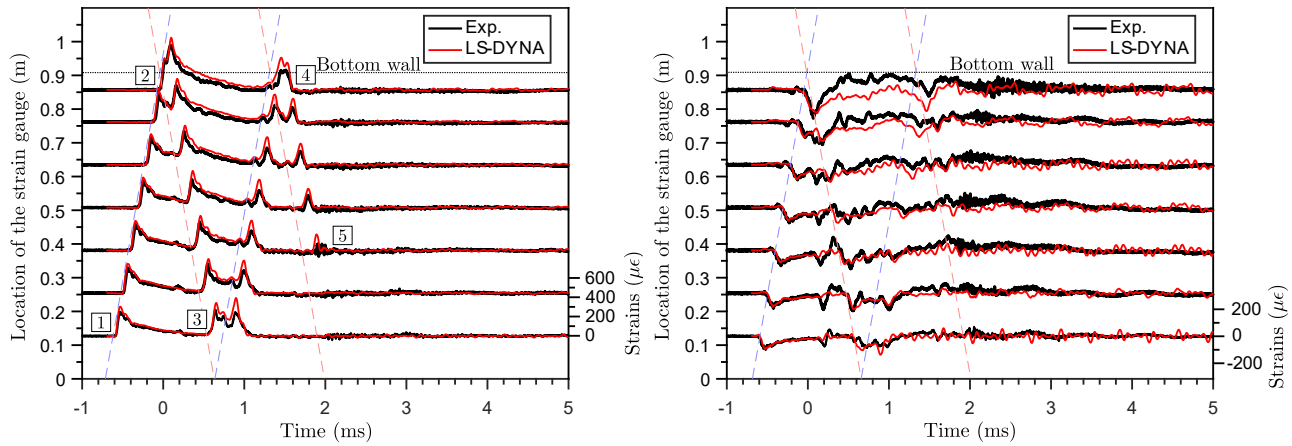

(a) Hoop strains

(b) Axial strains

Fig. 7: Hoop and axial strains for case 1.

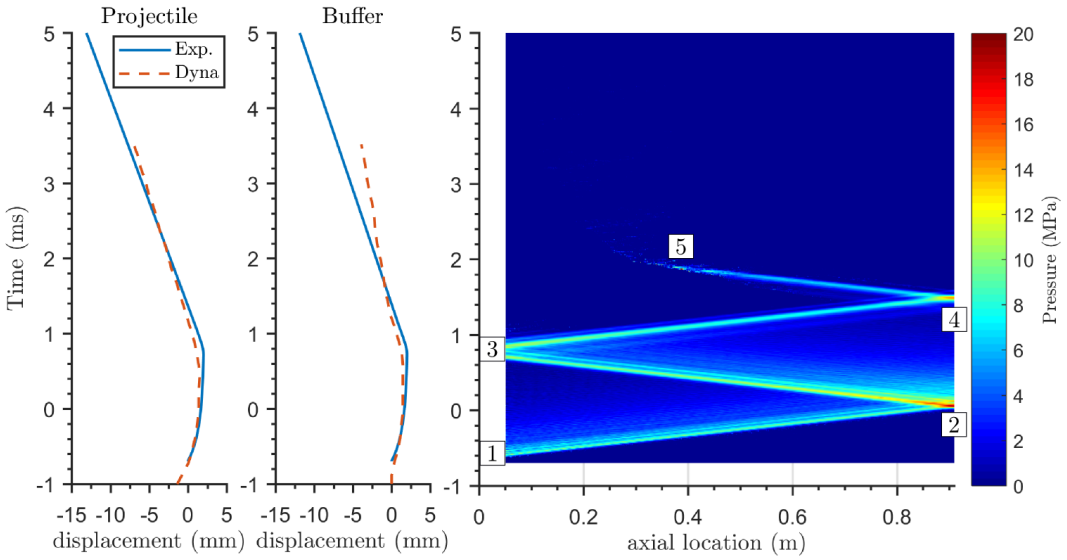

Fig. 8: Motion of the buffer and the projectile with a space-time pressure plot (LS-DYNA) for case 1.

and is related to the incident pressure ΔP_i by acoustic theory as:

$$\Delta P_r = \left[\frac{(\rho a)_2 - (\rho a)_1}{(\rho a)_2 + (\rho a)_1}\right] \Delta P_i \,. \tag{1}$$

For the present experiment, medium 1 is water and medium 2 is aluminum: $\Delta P_r \approx 0.82 \Delta P_i$. When the incident wave reflects at the bottom wall, the pressure there is the sum of the incident and the reflected waves, that is 1.82 ΔP_i in the present case or $\approx$ 15.6 MPa[3].

Pressures P1 and P2 are shown in Fig. 5. Note that all pressures in this paper are indicated as relative pressures. Both P1 and P2 are very similar in trend and magnitude; this is because there is no converging section and both pressure transducers are located only 50 mm apart. The peak pressure measured experimentally is 16.0 MPa, within 3% of the 15.6 MPa predicted using acoustic theory, and the peak pressure predicted with LS-DYNA is within 10% of the experimental value. The first pressure wave is followed by a second wave of smaller amplitude (reaching the bottom at $\sim$1.4 ms), and this is immediately followed by a first cavitation event. The cavitation event approximately spans from 2 ms to 31 ms (note the time-axis in Fig. 5 is discontinuous). This is followed by a few more cavitation events of decreasing duration and intensity (not shown and discussed in this paper, see [15] for more information).

The wave dynamics in the test specimen are further explained using Fig. 6. Upon impact of the projectile on the buffer (event 1), a stress (pressure) wave is produced in the liquid. This wave travels down the tube, partially reflects off the bottom wall (event 2) and then travels upward. After one round trip in the tube, the stress wave partially re-

[3]When the polycarbonate base fixture is used the sum of the incident and the reflected wave is 1.23 ΔP_i. This is a consequence of the lower acoustic impedance of polycarbonate compared to aluminum.

flects on the buffer (event 3). The reflection of the wave on the buffer produces a second stress wave which later reaches the bottom of the tube (event 4). The reflection of the stress wave on the buffer (event 3) also initiates an upward motion of the buffer. The upward motion of the buffer produces tension waves which immediately follow the second stress wave. The tension waves result in distributed cavitation in the water column (visual confirmation of this is provided in case 2). This cavitation event ends after the direction of motion of the buffer is once more reversed; the downward motion of the buffer sends a compression wave which collapses the bubbles as it propagates from top to bottom. The arrival of this compression wave at the bottom of the tube is detected by the pressure transducers (event 6).

This is followed by several cycles of cavitation (over much longer times than shown in the figures of this paper) of decaying duration and intensity. This is similar to what was observed and reported by Inaba and Shepherd [15, 16]. Note that the main focus of this paper is on the events which take place *early on* after the impact of the projectile on the buffer (i.e., events 1 thru 5).

The hoop (ε_θ) and axial (ε_z) strains from the experiment and the simulations are shown in Fig. 7 for the first 5 ms after impact. The bottommost trace corresponds to location S1, and the topmost trace corresponds to location S7 as summarized in Tab. 2. The scale for the strains is shown to the right of the plot.

The oblique lines shown in Fig. 7 have a slope which corresponds to the Korteweg speed c. The Korteweg speed is the expected velocity of the pressure waves in the liquid for the fluid-structure coupled problem in the absence of cavitation. It can be evaluated as follows:

$$c = \frac{a}{\sqrt{1+\beta}}\,, \tag{2}$$

where a is the sound speed in water, and $\beta = KD/(Eh)$ is the FSI coupling parameter with K the bulk modulus of water, D the average of the inner and outer diameter of the aluminum tube, E the Young's modulus of the tube, and h the thickness of the tube wall [16]. In the present case, $c = 1350$ m/s. Both liquid pressure waves and strains appear to propagate with the Korteweg speed.

Returning to Fig. 7, there is reasonable agreement between the experiment and the simulations, especially for the hoop strains. The axial strains predicted by LS-DYNA close to the bottom of the test specimen are not in good agreement with the experiment, which could be due to the sensitivity of the axial strains to the boundary conditions. The base fixture and the plates to which it is bolted are not modeled in detail, but the tube end is treated as fixed in the simulations. On the contrary, the boundary conditions applied on the top end of the tube are modeled realistically, allowing motion in both radial and axial directions. There, the agreement between the axial strains from the experiment and the simulation is much better than in the vicinity of the bottom end, close to the base fixture.

Figure 8 is a space-time plot of the pressure along with the motion of the projectile and the buffer. The measured and simulated motions of the projectile and buffer are in good agreement up to 2 ms. The space-time plot of the pressure from the simulation illustrates the propagation of the pressure wave along the axis of symmetry of the tube.

The dynamics of the transient behavior is now examined using Figs. 7a and 8. At approximately t = -0.6 ms (event 1), the projectile impacts on the buffer. This pushes the buffer down and generates a pressure wave within the liquid as described above. This pressure wave, the first incident wave, propagates downward into the liquid at the Korteweg speed of 1350 m/s (i.e., parallel to the characteristic lines shown in Fig. 7a). When the wave reaches the bottom of the tube at approximately t = 0 ms (event 2), reflection produces a wave traveling upward which will be called the first reflected wave.

The hoop strains created by the first incident and reflected pressure waves are approximately 300 $\mu\varepsilon$, except close to the bottom wall where the hoop strains are close to 600 $\mu\varepsilon$ due to the pressure increase associated with reflection.

When the first reflected wave reaches the bottom end of the buffer, it reflects (event 3) producing the second incident wave traveling downward into the liquid. This wave, however, is *immediately* followed by tension waves due to the motion of the buffer. This is because upon reflection of the first reflected wave on the buffer (event 3), the liquid pressure below the buffer is large. The resulting force applied on the buffer accelerates the latter upward, and this upward motion produces tension waves just behind the second incident wave. Those tension waves also explains why the second reflected wave (the one produced during event 4) is eventually annihilated (event 5).

Regarding the axial strains, assuming zero axial stress[4] and using shell theory yields $\varepsilon_z = -\nu\varepsilon_\theta$ [21]. This implies the axial strains are produced through the Poisson effect. Using the experimental results it is possible to verify that the relation above is approximately satisfied; the magnitude of the axial strains is approximately one-third that of the hoop strains.

4.2 Case 2

Case 2 is identical to case 1, except the test was performed using the aluminum base fixture which has a cone. The impact velocity of the projectile on the buffer is 5.6 m/s. Acoustic theory, as introduced earlier, predicts a peak pressure of 15.3 MPa at the bottom of the test specimen. However, shock focusing could occur within the cone [22], and this could result in a larger peak pressure at the tip (P2) [8].

Pressures P1 and P2 are shown in Fig. 9. We recall that transducer P1 is mounted above the cone, and transducer P2 is mounted at the apex of the cone. The maximum value of P1 and P2 is 14.8 MPa which is in reasonable accord with the predicted value of 15.29 MPa. The fact that the peak pressures recorded above the cone (P1) and at the tip of the

[4] This assumption is only valid close to the top end of the tube.

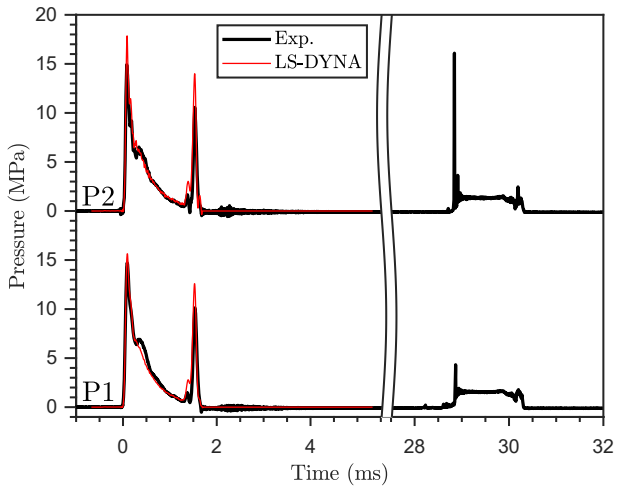

Fig. 9: Pressure at the bottom end for case 2 (the time axis is discontinuous).

cone (P2) are similar suggests that shock focusing does not occur.

Shock focusing did not occur in this test because the round trip time $2l/a$ for pressure waves within the converging section is $\sim$ 24 μs, compared to to the rise time of the first incident pressure wave of approximately 100 μs. The pressure has time to equilibrate throughout the cone during pressurization (i.e., the pressure is approximately spatially uniform), and shock focusing does not occur.

Pressures P1 and P2 due to the collapse of the cavitation bubbles, 29 ms after impact, are substantially different. The peak pressure above the cone (P1) is 4.3 MPa, and the peak pressure at the tip of the cone (P2) is 16.1 MPa. In repeat tests, the peak pressure measured at the tip of the cone was consistently higher than the peak pressure measured above the cone.

The explanation of the larger pressure at the tip of the cone is twofold. First, shock focusing can occur [22]. The rise time of the pressure wave is approximately 10 μs, and this is less than the acoustic transit time of the waves within the cone. The pressure is not uniform throughout the cone during pressurization, and amplification of the pressure is possible (see Veilleux and Shepherd [8]). Second, the collapse of bubbles within the cone can be enhanced by the geometry. This is discussed by Veilleux *et al* [23] who found that focusing of the pressure waves on the axis of symmetry can accelerate the collapse of bubbles.

The strains for case 2 are not shown; they are very similar to the strains for case 1; the wave dynamics within the test specimen is the same as for case 1, except locally in the cone. The strains we measured are however insensitive to the local effect of the cone due to the placement of the gauges away from this region.

Case 2 was also repeated a number of times with the polycarbonate base fixture in order to observe bubble dynamics in the cone. The timing of the events and the magnitude of the peak pressures are very similar to those obtained with the aluminum base. A sequence of frames obtained with the polycarbonate base fixture is shown in Fig. 10. The time stamp shown at the top of each frame should be used to approximately locate each frame on the pressure history shown in Fig. 9 (we recall that Fig. 9 was obtained with an *aluminum* base fixture). The edges of the straight tube and the cone are identified in the first frame of Fig. 10.

The first two frames (t = -1.0 ms and t = 1.0 ms) show no sign of cavitation. This is expected since no tension waves have reached the bottom end of the tube yet, and this region is under compression (i.e., $P > 0$ MPa). The first tension waves reach the bottom of the tube at t = 1.8 ms, and we observe the nucleation of several bubbles distributed throughout the visible portion of the tube. The polycarbonate base fixture introduces astigmatism along the optical path, and it is only possible to clearly distinguish the bubbles forming on the front of the tube. The bubbles forming away from the front are visible, but out of focus.

From t = 3.0 ms to t = 18.8 ms we observe the growth of multiple bubbles. In particular, a few bubbles forming and growing in the cone coalesce to produce a larger bubble approximately centered on the axis of symmetry, and located deep into the cone. The collapse of the bubbles takes place from t = 20.8 ms to t = 28.8 ms. The bubbles successively collapse from top to bottom due to the slow progression of a compression wave in the bubbly mixture. The collapse of the bubbles is asymmetric, as expected, due to the proximity of the walls and the shock induced origin of the collapses [24].

4.3 Case 3

Case 3 is identical to case 1, except there is a "small", 3.5 mm, air gap between the bottom of the buffer and the water surface. The impact velocity of the projectile on the buffer is 5.5 m/s. The air gap drastically affects both the interaction of the projectile and buffer, as well as the transmission of pressure waves into the liquid column.

Pressures P1 and P2 are shown in Fig. 11 for the first 5 ms after impact. The dynamics taking place after 5 ms is very similar to what was observed and described using cases 1 and 2. Once more, the signals recorded using P1 and P2 are very similar in trend and magnitude. The pressure history is however more complicated than it was in cases 1 and 2; there are now multiple pressure peaks. The measured peak pressure is approximately 11.0 MPa; 30% lower than the peak pressures measured for case 1. This is because the water column is now pressurized through the isentropic compression of the air gap. LS-DYNA does not predict all the fine details of the experimental pressure traces, but it does predict the presence of multiple pressure peaks.

The motion of the projectile and the buffer along with a space-time plot of the pressure is shown in Fig. 12. The projectile bounces off the buffer resulting in multiple impacts between the projectile and the buffer, which is different from cases 1 and 2 where only one impact was observed. When there is an air gap, the projectile, the buffer and the air gap form a spring-mass system with the air gap being equivalent to a non-linear spring. Although the results are not presented here, using rigid body mechanics (i.e., conservation

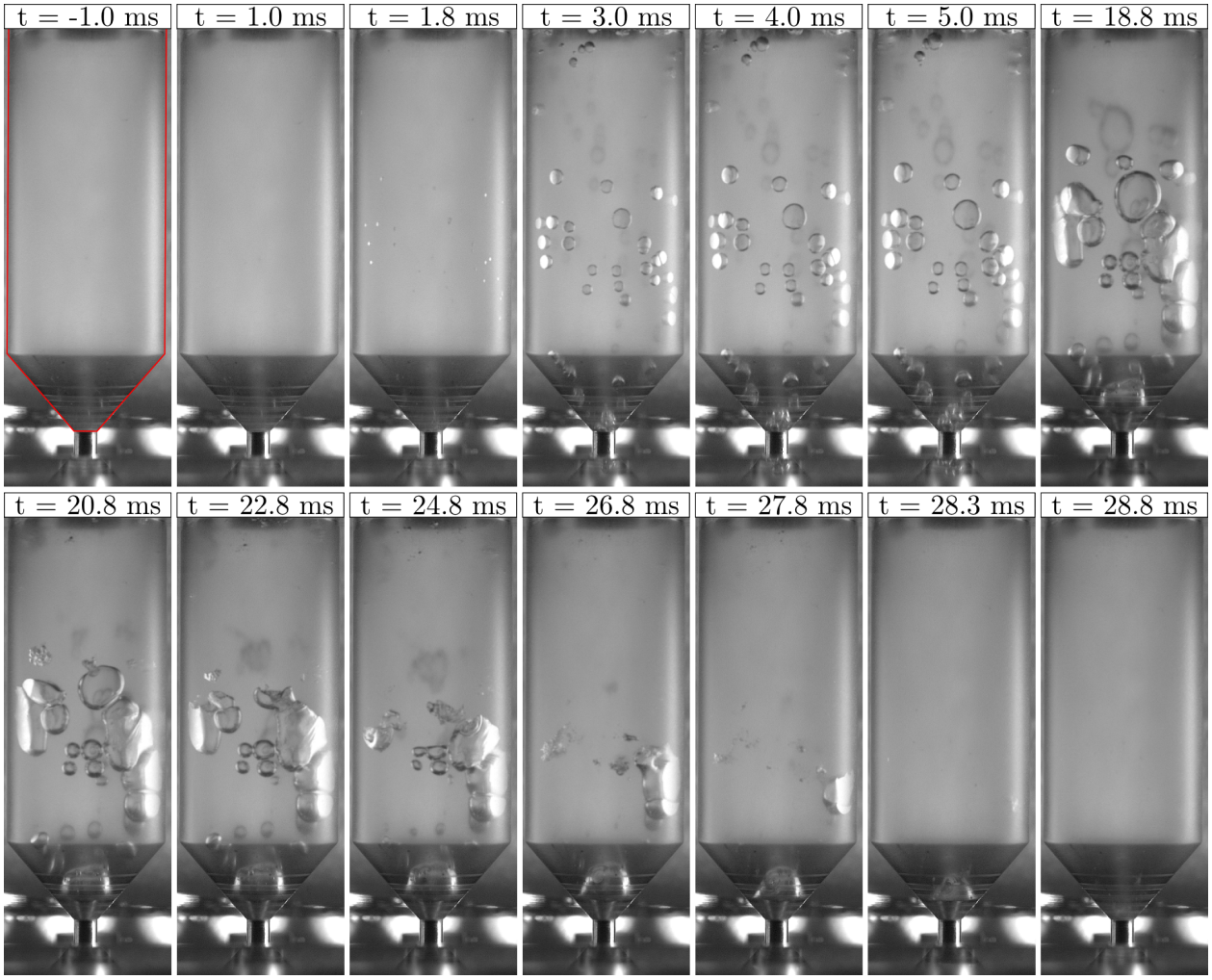

Fig. 10: Sequence of images showing distributed cavitation for case 2.

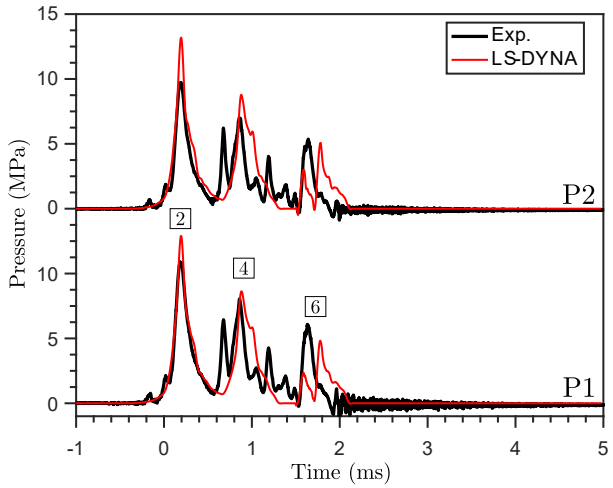

Fig. 11: Pressure at the bottom end for case 3.

of momentum and energy) with a non-linear spring for the air gap enables reasonable quantitative predictions of the interactions between the projectile, the buffer and the air gap. It is possible to approximate the pressure within the air gap as uniform since the waves transit sufficiently rapidly (10 μs) within the air gap that there are multiple reverberations during the compression or the expansion of the gap.

There are now 3 distinguishable impacts between the projectile and the buffer (events 1, 3 and 5), each of which results in the production of a pressure wave. Each of these waves will reflect at the bottom wall (events 2, 4 and 6) and propagate upward, toward the buffer. However, only the wave due to the first impact has enough time to reach the top of the liquid column. This is because the reflection of the first compression wave (event 5) happens at a free surface and this produces a tension wave. This can be understood using Eq. 1: medium 1 is water and medium 2 is air. The acoustic impedance of air is negligible compared to the acoustic impedance of water. Therefore, $\Delta P_r \approx -\Delta P_i$: the sign of the pressure wave changes, and a compression wave becomes a tension wave upon reflection.

As in case 1, the buffer starts moving upward after reflection occurs (event 5), and this creates relatively strong tension waves. The tension waves produced at the top end of the tube will propagate throughout the tube and interfere destructively with the second and third waves before they reach the buffer. At t = 2.5 ms (event 8), the entire water

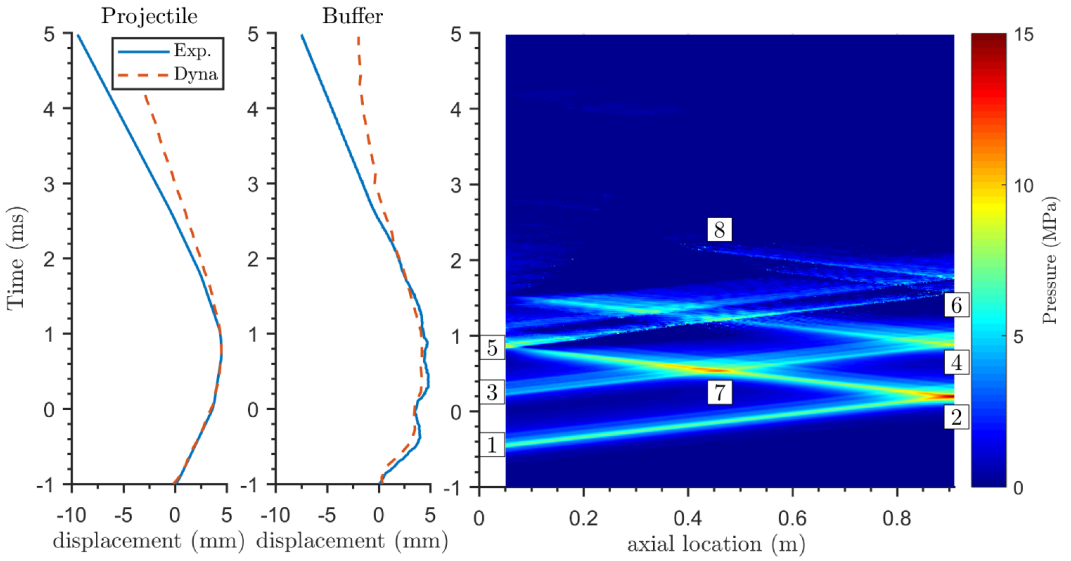

Fig. 12: Motion of the buffer and the projectile with a space-time pressure plot (LS-DYNA) for case 3.

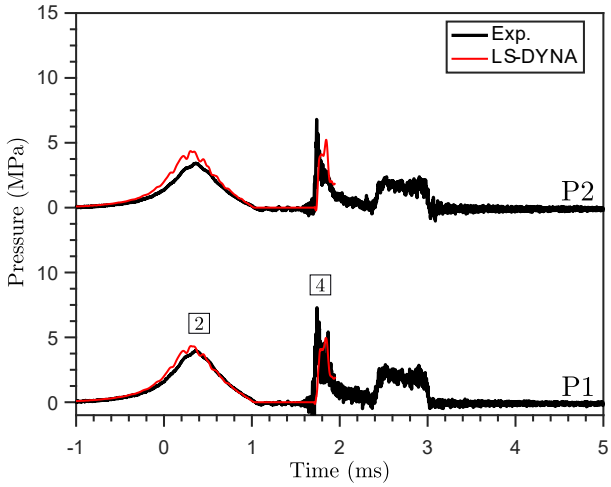

Fig. 13: Pressure at the bottom end for case 4.

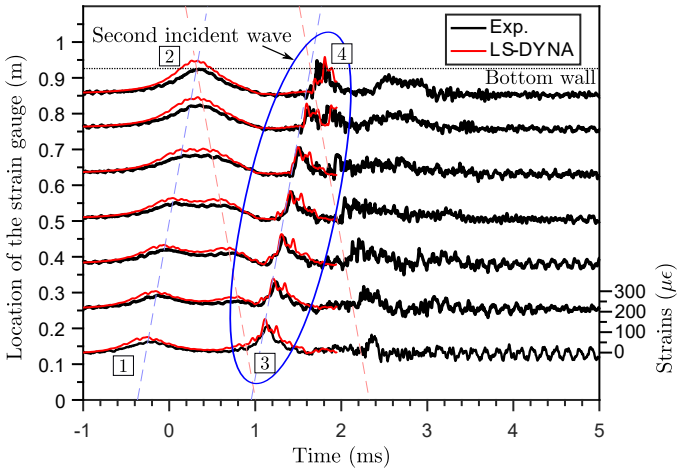

Fig. 14: Hoop strains for case 4.

column is under the influence of the tension waves, and distributed cavitation occurs: this is identical to what happens in cases 1 and 2, and this was also observed by Inaba and Shepherd [15]. Images of the distributed cavitation are not included since the cavitation event is qualitatively similar to the one reported for case 2.

Another interesting feature is the possibility of having some constructive interference between the multiple waves propagating within the tube. This is observed at event 7 where the incident wave due to the second impact interacts constructively with the reflected wave due to the first impact. The constructive interference can result in peak pressures and strains in locations away from the bottom of the tube.

4.4 Case 4

Case 4 is identical to case 3 except there is initially a "large", 12.0 mm air gap between the buffer and the water surface. The impact velocity of the projectile on the buffer is 5.6 m/s. The size of the air gap drastically affects the timing of the multiple impacts between the projectile and the buffer.

Pressures P1 and P2 are shown in Fig. 13 up to 5 ms after impact. The two pressure traces are again very close in trend and magnitude. The match between the experiment and the simulation is also good. It is now possible to distinguish two main pressure waves. The first one reaches a peak pressure of approximately 3.9 MPa at t = 0.3 ms, and the pressurization happens slowly in comparison to the wave transit times through either gas or liquid; the pressure takes $\sim$ 1 ms to reach its peak value. The second pressure wave is very sharp and reaches a peak value of 7.2 MPa at t = 1.75 ms. The rise time associated with this pressure wave is approximately 30 μs. Between the first and the second pressure waves (t between 1.0 and 1.6 ms), the liquid is under the influence of tension waves, and cavitation occurs. Unlike cases 1 and 2, the second pressure wave is *not* due to the reflection of the first pressure wave.

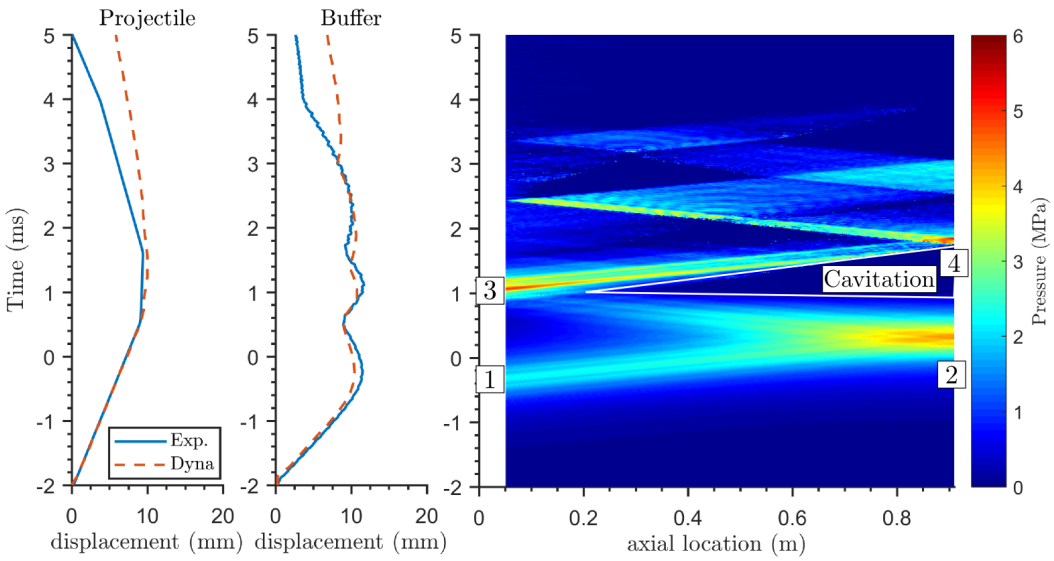

Fig. 15: Motion of the buffer and the projectile with a space-time pressure plot (LS-DYNA) for case 4.

The projectile and buffer's motion along with a space-time plot of the pressure are shown in Fig. 15. There are multiple impacts between the projectile and the buffer. The first one (event 1) produces the slow pressurization of the water column through compression of the air gap. This corresponds to the first pressure pulse visible on both P1 and P2. When this first wave reflects off the bottom wall (event 2), a compression wave traveling upward is produced. When this wave reaches the top of the tube and reflects off the free surface between the air and the liquid, it becomes a tension wave for the same reason as in case 3, and it causes distributed cavitation. This tension wave is followed by the second incident wave, which is produced by the second impact of the projectile on the buffer (event 3). This second incident wave is propagating into a bubbly mixture created by the cavitation resulting from the tension wave.

The effective sound speed in a cavitating liquid (i.e., a two phase mixture) is a strong function of the void fraction [24]. The collapse of the cavities under pressure will reduce the void fraction, increase the wave speed, and result in wave steepening. This results in the second incident pressure wave becoming a shock wave before reaching the bottom end of the tube. This explains the very short rise time of the second pressure wave (see Tab. 3).

The steepening of the second pressure wave is also observed on the hoop strains shown in Fig. 14. For stations S3 to S7, careful reading of the plot shows that the second incident wave is preceded by a negative hoop strain which indicates the liquid is locally at a sub-atmospheric pressure. Visually, the steepening of the wave is observed between locations S3 to S7. The rise times of the hoop strains and pressures associated with the second incident wave are summarized in Tab. 3.

LS-DYNA simulates the steepening of the pressure wave despite the absence of an explicit cavitation model. As mentioned previously, this is because of the boundary condition between the aluminum tube and the water which mimics the effect of cavitation. We confirmed that by using a boundary condition which allows for tensile forces between the two surfaces eliminates the steepening of the wave.

Table 3: Rise time of the second incident wave.

Station	S1	S2	S3	S4	S5	S6	S7	P1	P2
T (μs)	360	170	160	130	70	70	50	30	30

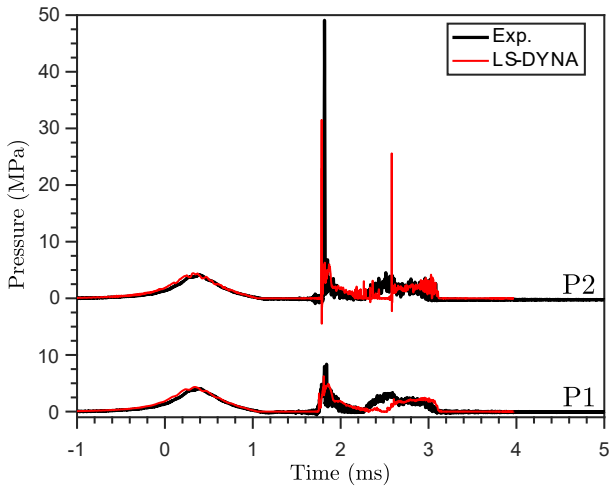

Fig. 16: Pressure at the bottom end for case 5.

4.5 Case 5

Case 5 is identical to case 4, except the test specimen is terminated with a converging section. The impact velocity of the projectile on the buffer is 6.4 m/s. The dynamics of cases 4 and 5 are identical; only the pressure at the bottom of the test specimen differs between these cases.

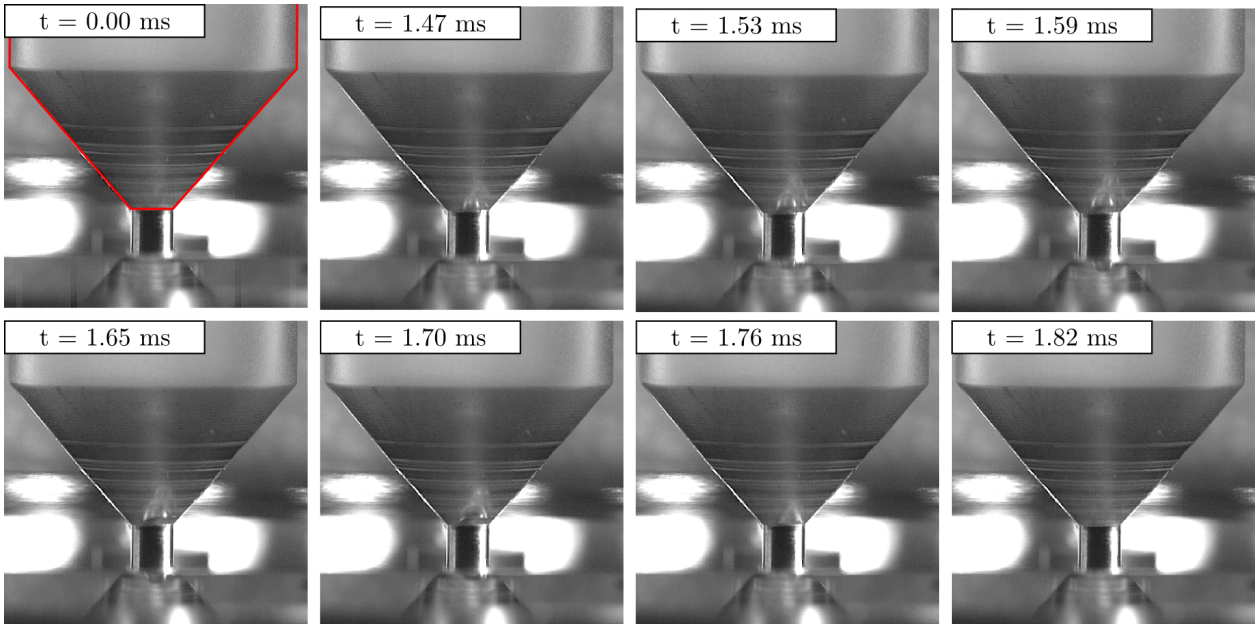

Fig. 17: Sequence of images showing cavitation at the tip of the cone for tests performed with a large air gap.

Both P1 and P2 are shown in Fig. 16. As in case 4, there are two main pressure waves produced by the impacts between the projectile and the buffer. We first consider the first wave which has a rise time of order $\sim$ 1 ms. The peak pressure is approximately 4.3 MPa, and it is well predicted by LS-DYNA. The peak pressure due to the first wave is the same above the cone (P1) and at the tip of the cone (P2); there is no amplification of the pressure due to the converging section. There is no shock focusing because the transit time of the acoustic waves in the cone (24 μs) is short compared to the 1 ms rise time of the first pressure wave. The rise time of the second pressure wave is approximately 16 μs (measured using P2). The peak pressure measured at the apex of the converging section (P2) is approximately 50 MPa, and the peak pressure measured above the converging section (P1) is about 8.4 MPa.

Identical to case 2, the explanation for the larger peak pressure at the tip of the cone is twofold. First, there is shock focusing within the cone [22]. Shock focusing is possible because the rise time of the pressure wave (16 μs) is less than the acoustic transit time of the waves within the cone (24 μs). The strain signals for case 5 (not shown in this paper) are similar to those shown for case 4. Wave steepening is observed and responsible for the short rise time of the second pressure wave, which makes shock focusing possible. Second, there is a rapid bubble collapse within the cone in the vicinity of the tip where the pressure transducer is mounted.

Repeated tests were performed with the same experimental conditions as case 5, but the aluminum base fixture was replaced with the polycarbonate base fixture, making it possible to visualize the cavitation event in the cone. The timing of the events and the magnitude of the peak pressures with the polycarbonate base fixture is similar to what was obtained with the aluminum base fixture. There is however one significant physical difference: wave steepening does not occur when the polycarbonate base fixture is used.

The absence of wave steepening results from a milder distributed cavitation event in the tube when the polycarbonate fixture is used. The steepening of the second incident wave, as explained earlier using case 4, is caused by the propagation of the second incident wave in a bubbly mixture due to cavitation. If the cavitation event is milder there are less bubbles and/or they remain smaller, resulting in less or no steepening at all of the second incident wave as it propagates down the tube.

The milder distributed cavitation event in the tube terminated with the polycarbonate fixture is due to the lower acoustic impedance of polycarbonate ($\approx$ 3 MPa·s/m) compared to aluminum ($\approx$ 15 MPa·s/m). With the aluminum base fixture, 82% of the first incident wave is reflected at the bottom wall, compared to 23% with the polycarbonate base fixture. We recall that the reflected part of the first incident wave, upon reaching the interface between the liquid and the air gap, becomes a tension wave, and this is what creates the tension wave responsible for the cavitation event. The reduction in the magnitude of the reflected wave indicates that the magnitude of the tension wave is less, thus causing a milder cavitation event.

Figure 17 is a sequence of images of the cavitation event in the cone. The polycarbonate base fixture was used to obtain this sequence of images. The time stamps shown at the top of each frame can be used to approximately position each frame on the pressure history shown in Fig. 16 (we recall that Fig. 16 was obtained with an *aluminum* base fixture).

The first frame (i.e., t = 0.00 ms) was taken before the arrival of the tension wave at the bottom of the tube, and there is no cavitation. The frames from t = 1.47 ms to t = 1.59 ms show the growth of a cavitation bubble. The bubble appears to nucleate in the vicinity of the tip of the cone, where the pressure transducer is located. The collapse of the bubble

is shown with the frames t = 1.65 ms to t = 1.82 ms. The collapsing bubble remains close to the pressure transducer, which explains partially the larger peak pressure recorded at the tip of the cone compared to the peak pressure recorded above the cone.

5 Conclusion

The impulsively-generated pressure and strain transients inside a cylindrical, fluid-filled tube were studied experimentally and numerically. The effect of an air gap and a converging section were studied using five cases.

Case 1, the simplest case, has no air gap and no converging section. It was found that the upward motion of the buffer upon reflection of the pressure wave on the buffer produces tension waves, and this causes distributed cavitation to occur.

Case 2 is identical to case 1, except there is a converging section at the bottom end of the tube. No shock focusing of the primary pressure wave generated upon the impact of the projectile on the buffer was observed. The peak pressure recorded upon collapse of the cavitation bubbles was however found to be much larger at the tip of the cone than above the cone. The amplification is due to a combination of shock focusing and the effect of the cone on the collapsing bubble.

Case 3 has the same geometry as case 1, but a small air gap was introduced between the buffer and the water. The presence of an air gap drastically affects the dynamics of the projectile and buffer; there are now multiple collisions between the projectile and the buffer resulting in multiple pressure waves within the tube. Constructive interference between the waves is observed.

Case 4 is identical to case 3, except the air gap is large. The size of the air gap drastically affects the timing of the multiple impacts between the projectile and the buffer. As a result, the wave generated through the second impact propagates in a cavitating liquid, and wave steepening leading to shock waves is possible.

Case 5 is identical to case 4, except there is a converging section at the bottom end of the tube. The pressure measured at the tip of the cone is substantially larger than the pressure measured above the cone. The amplification of the pressure is due to a combination of shock focusing and the rapid collapse of a bubble in the immediate vicinity of the pressure transducer.

The material used to fabricate the base fixture terminating the tube affects the wave dynamics in the liquid. Materials of lower acoustic impedance, such as polycarbonate, result in reflected waves of lesser magnitude. In some cases this can result in milder cavitation events in the liquid, suppressing wave steepening.

It is not possible to directly extrapolate the results with the stationary scale model to autoinjector devices as there are many important features which are not simulated by the simple experimental fixture discussed in this paper. The present study is part of a larger research program that used actual devices, more complex models and numerical simulation to address that question (see the discussion in Veilleux and Shepherd [8]).

Using the insights from our other investigations, we can draw some preliminary conclusions from the pressure and strain measurements reported above. The measured stains away from the cone region (Figs. 7 and 14) and the peak pressure measured within the cone for cases 1 to 4 imply maximum principal stresses which are too small to explain initiation of fractures in devices even accounting for the non-similarity of the fixture including possible stress concentrations in the cone region or at the shoulder of the syringe. However, the very high peak pressures (50 MPa in Fig. 16) observed in case 5 indicate that shock focusing and cavitation bubble collapse, either alone or in concert, have the potential of causing localized stresses that could initiate fractures in the cone region. Because the pressure loading is very localized and transient, this results in an unsteady, three-dimensional stress field which has to be investigated through numerical simulations, which has been done and will be reported in future publications.

The important effect of the syringe motion on the pressure and stress transients will be reported in a separate publication. The use of dampers to mitigate the peak magnitude of the pressure and stress transients has been examined. Experimental results have confirmed that foam dampers introduced inside the device can reduce the peak pressure and strains by 50 % or more [25].

Acknowledgements

This work is sponsored by Amgen through the Caltech-Amgen Research Collaboration Agreement for Chem-Bio-Engineering Awards.

References

[1] Akers, M. J., 2010. *Sterile Drug Products: Formulation, Packaging, Manufacturing and Quality*, 1st ed. CRC Press, Boca Raton.

[2] Limmroth, V., and Gerbershagen, K., 2014. "Single-use autoinjector for once-weekly intramuscular injection of IFNβ-1a.". *Expert Opin. Drug Deliv.,* **11**(12), p. 1969. DOI:10.1517/17425247.2014.943181.

[3] Schiff, M., Jaffe, J., Freundlich, B., and Madsen, P., 2014. "New autoinjector technology for the delivery of subcutaneous methotrexate in the treatment of rheumatoid arthritis.". *Expert Rev. Med. Devices,* **11**(5), pp. 447–455. DOI: 10.1586/17434440.2014.929492.

[4] Thompson, I., and Lange, J., 2013. "Pen and Autoinjector Drug Delivery Devices". In *Sterile Product Development: Formulation, Process, Quality and Regulatory Considerations*, P. Kohle, M. Shah, and N. Rathore, eds., AAPS Advances in the Pharmaceutical Sciences Series. Springer-Verlag New York, pp. 331–356. DOI: 10.1007/978-1-4614-7978-9.

[5] Lange, J., and Thompson, I., 2013. "Self-Injection Devices". In *Encyclopedia of Pharmaceutical Science and*

Technology, J. Swarbrick, ed., 4^{th} ed. CRC Press, Boca Raton, pp. 3132–3143.

[6] Thompson, I., 2006. "Self-Injection Technology and Trends". *J. Innovations in Pharmaceutical Technology,* **20**, pp. 60–63.

[7] French, D., and Collins, J., 2010. "Advances in Parenteral Injection Devices and Aids". In *Pharmaceutical Dosage Forms: Parenteral Medications*, S. Nema and J. Ludwig, eds., 3rd ed. Informa Healthcare, pp. 71–85.

[8] Veilleux, J.-C., and Shepherd, J., 2018. "Pressure and Stress Transients in Autoinjector Devices". *Drug Deliv. and Transl. Res.* DOI: 10.1007/s13346-018-0568-7.

[9] Fry, A., 2014. "Injecting Highly Viscous Drugs". *Pharmaceutical Technology,* **38**(11).

[10] Stout, D., and Vilivalam, V., 2009. "Plastic Prefilled Syringes: A Better Fit for Autoinjector Systems". *Pharmaceutical Technology*. Volume 2009 Supplement, Issue 6.

[11] Wiggert, D. C., and Tijsseling, A., 2001. "Fluid transients and fluid-structure interaction in flexible liquid-filled piping.". *Appl. Mech. Rev.,* **54**(5), pp. 455–481. DOI: 10.1115/1.1404122.

[12] Wylie, E., and Streeter, V., 1993. *Fluid Transients in Systems*. Prentice Hall, Englewood Cliffs, NJ.

[13] Watters, G. Z., 1984. *Analysis and Control of Unsteady Flow in Pipelines.*, 2nd ed. Butterworths, Stoneham, MA.

[14] Bergant, A., Simpson, A., and Tijsseling, A., 2006. "Water hammer with column separation: A historical review". *J. Fluids Struct.,* **22**. DOI: 10.1016/j.jfluidstructs.2005.08.008.

[15] Inaba, K., and Shepherd, J. E., 2010. "Dynamics of Cavitating Flow and Flexural Waves in Fluid-Filled Tubes Subject to Axial Impact". In Proceedings of the ASME 2010 Pressure Vessels & Piping Division. Paper PVP2010-25989.

[16] Shepherd, J. E., and Inaba, K., 2010. "Shock Loading and Failure of Fluid-Filled Tubular Structures". In *Dynamic Failure of Materials and Structures*, G. Ravichandran and Y. Rajapakse, eds. Springer-Verlag US, pp. 153–190. DOI: 10.1007/978-1-4419-0446-1.

[17] J. O. Hallquist, 2016. *LS-DYNA : THEORY MANUAL*, latest ed. Livermore Software Technology Corporation, Livermore, California (USA). `http://www.lstc.com`.

[18] Wu, Z., Zong, Z., and Sun, L., 2014. "A Mie-Grüneisen mixture Eulerian model for underwater explosion.". *Eng. Computations,* **31**(3), pp. 425–452.

[19] Kojima, T., Inaba, K., Takahashi, K., Triawan, F., and Kishimoto, K., 2017. "Dynamics of Wave Propagation Across Solid-Fluid Movable Interface in Fluid-Structure Interaction". *J. Pressure Vessel Technol.,* **139**(3), pp. 031308–031308–9. DOI: 10.1115/1.4035376.

[20] Liepmann, H. W., and Roshko, A., 2001. *Elements of gasdynamics.* Dover Publications, Mineola, NY.

[21] Bitter, N. P., and Shepherd, J. E., 2013. "On the Adequacy of Shell Models for Predicting Stresses and Strains in Thick-Walled Tubes Subjected to Detonation Loading". In Proceedings of the ASME 2013 Pressure Vessels & Piping Division. Paper PVP2013-97148. DOI: 10.1115/PVP2013-97148.

[22] Sturtevant, B., and Kulkarny, V. A., 1976. "The focusing of weak shock waves". *Journal of Fluid Mechanics,* **73**(4), p. 651671.

[23] Veilleux, J.-C., Maeda, K., Colonius, T., and Shepherd, J. E., 2018. "Transient Cavitation in Pre-Filled Syringes During Autoinjector Actuation". In Proceedings of the 10th International Symposium on Cavitation.

[24] Brennen, C. E., 2013. *Cavitation and bubble dynamics.* Cambridge University Press, Cambridge. DOI: 10.1017/CBO9781107338760.

[25] Veilleux, J.-C., and Shepherd, J. Dampers and methods for performing measurements in an autoinjector. US Patent Application 20180015224. Filed July 2017. Published January 2018.